CrystEngComm

COMMUNICATION

View Article Online
View Journal | View Issue

Cite this: *CrystEngComm*, 2016, **18**, 2244

Received 2nd December 2015,
Accepted 29th February 2016

DOI: 10.1039/c5ce02355f

www.rsc.org/crystengcomm

Synthesis of single-crystalline $Ge_1Sb_2Te_4$ nanoplates in solution phase†

Wei-Hsiang Huang,‡[a] Tzu-Lun Gao,‡[a] Chun-Wei Huang,[b] Chia-Fu Chang,[b] Wen-Wei Wu*[b] and Hsing-Yu Tuan*[a]

A chemical route to synthesize single-crystalline $Ge_1Sb_2Te_4$ (GST-124) hexagonal nanoplatelets is reported, showing the first example of obtaining colloidal GeSbTe nanoalloys in solution phase.

Ternary alloys of chalcogenide nanomaterials have stimulated considerable interest due to their unique electrical, optical, and phase-change properties. Multiple dimensional nanostructured chalcogenides, such as $AgInS_2$, $CuInSe_2$, and GeSbTe, have been synthesized in vapor or solution phase *via* arrested precipitation, VLS growth, and template growth *etc.*[1–6] These nanomaterials have been used as building blocks for a variety of applications, including photovoltaic devices,[7,8] light-emitting diodes,[9] energy storage devices,[10] fluorescence biological imaging,[11] phase-change memories,[12] and thermoelectrics.[13]

Colloid synthesis in solution phase has the advantages of producing nanomaterials with various shapes and compositions and large production output. However, ternary GeSbTe (GST) types of nanostructures are yet to be synthesized in solution. The reported material related to the GST system is binary GeTe. For example, GeTe nanomaterials of various shapes, such as faceted octahedral single crystalline, cube-shaped, size-tunable and amorphous structures, were synthesized.[14–19] Therefore, how to synthesize ternary compositions of colloid GST nanomaterials remains a challenging issue to overcome.

Herein, we report the GST-124 hexagonal nanoplate synthesis, which represents the first example of ternary GST nanoalloys in the solution route. GST-124 nanoplates were synthesized using a Schlenk line system under an argon stream. GeI_4, $SbCl_3$ (or $Sb(OAc)_3$) and Te were dissolved separately in portions of the organic solution (OLA/OA/TOP/HMDS). Sb precursors, including $SbCl_3$ or $Sb(OAc)_3$, were added to induce the formation of ternary GST nanoplates. Each precursor solution was injected sequentially into OLA preheated to 130 °C (see the ESI† for experimental details). The reaction temperature was then increased to 320 °C at the rate of 2 °C per minute, and the solution was aged for 4 h to form the GST-124 nanoplates.

Fig. 1a shows the XRD patterns of the GST-124 nanoplates using $SbCl_3$ as the precursor during the synthesis. All the detected peaks in the XRD patterns are indexed as those from the rhombohedral GST-124 crystals [$(R\bar{3}m)$(166) space group] with hexagonal cells (Fig. 3b) and lattice constants a_0 = 0.427 nm and c = 4.06 nm (Fig. 1b), which are in agreement with those of the high-temperature phase (230 °C, hexagonal phase) at different annealing temperatures of the GST-124 film.[20]

Fig. 2a shows the SEM image of the GST-124 nanoplates using $SbCl_3$ as the precursor during the synthesis. The anisotropic growth phenomenon of the GST-124 nanoplates is likely ascribed to the presence of surfactants, including OLA, OA, and TOP capped on the surface of the nuclei, leading to the difference in surface energy; it may have also resulted from the crystal nucleation and growth mechanism as reported in other synthetic approaches, such as PVD,[21] MOCVD,[22,23] and bulk annealing.[24] Although GST-124

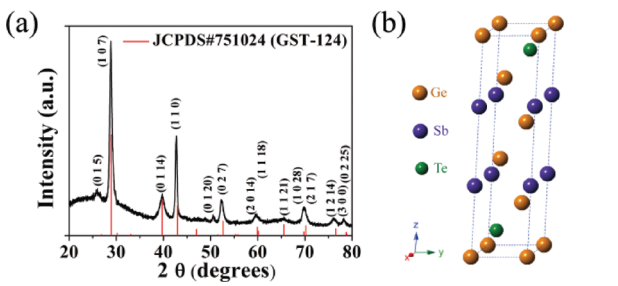

Fig. 1 (a) XRD analysis of the GST-124 nanoplates; the expected spectrum of the GST-124 stable phase is also shown (red line). (b) Simulated rhombohedral structure of GST-124.

[a] *Department of Chemical Engineering, National Tsing Hua University, Hsinchu 30013, Taiwan. E-mail: hytuan@che.nthu.edu.tw*
[b] *Department of Materials Science and Engineering, National Chiao Tung University, Hsinchu 30010, Taiwan. E-mail: wwwu@mail.nctu.edu.tw*

† Electronic supplementary information (ESI) available. See DOI: 10.1039/c5ce02355f

‡ These authors contributed equally to this work.

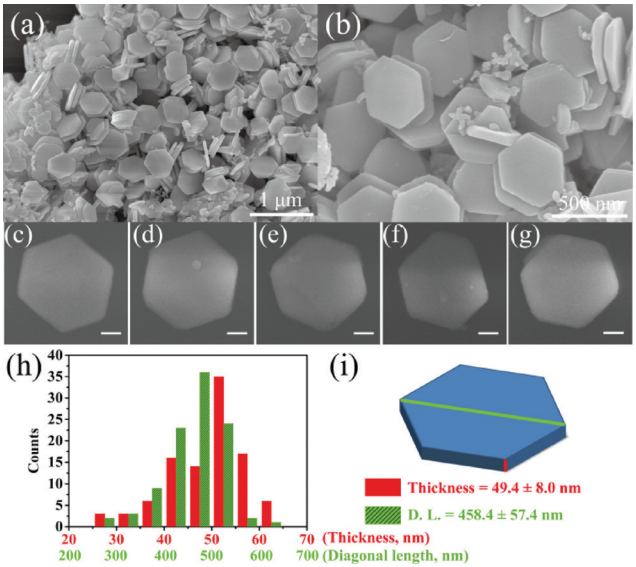

Fig. 2 (a and b) SEM images of as-prepared nanoplates using $SbCl_3$ as the Sb source. (c–g) Single GST-124 nanoplates. (h) Diagonal length and thickness distribution histogram of the nanoplates. (i) Schematic diagram of a single GST-124 nanoplate defining the diagonal length and thickness. Scale bar in (c–g), 100 nm.

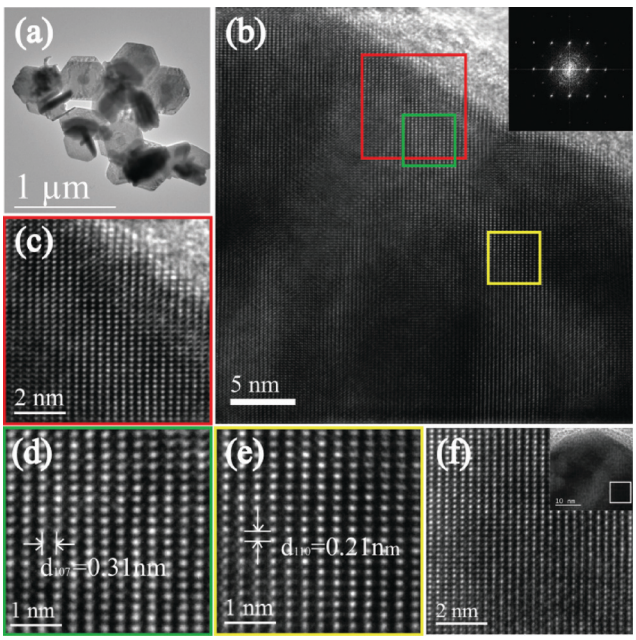

Fig. 3 (a) TEM image of a group of GST-124 nanoplates. (b–f) HR-TEM images at different positions of a single GST-124 nanoplate. Insets of (c–e): the corresponding FFT patterns of the HRTEM images with a zone axis of [$\bar{7}\bar{7}2$].

nanoplates tend to aggregate with themselves, the nanoplates can be segregated by spin-coating (Fig. 2c–g). The statistical results of the diagonal length and thickness distribution of the GST-124 nanoplates measured from the SEM images are 458.4 + 57.4 nm and 49.4 + 8.0 nm, respectively (Fig. 2h). A suitable precursor is important to form GST-124 nanoplates of high quality. Although using $Sb(OAc)_3$ as the precursor can also obtain GST nanoalloys, the product shapes are irregular and more self-aggregated (Fig. S1, ESI†), which is probably because the nucleation and growth are affected by the poor solubility of $Sb(OAc)_3$ in TOP.

To confirm the crystallographic and compositional properties of the GST-124 nanoplates, TEM and EDS investigations were performed. The TEM image of a group of GST-124 nanoplates is shown in Fig. 3a. The high resolution TEM (HRTEM) image of a single nanoplate shows a clear fringe. Images of different areas (Fig. 3c–f) inside a single GST-124 nanoplate show clear single crystalline nature (Fig. 3b–e), and the corresponding fast Fourier transform (FFT) patterns show the same results. The measured *d*-spacing of 0.31 nm between the adjacent lattice planes in Fig. 3d corresponds to the {107} planes and the measured *d*-spacing of 0.21 nm in Fig. 3e corresponds to the {110} planes. All chemical compositions are homogeneous throughout the GST-124 nanoplates as revealed by elemental mapping (Fig. 4). EDS quantitative analysis of different selected nanoplates confirmed that the composition is $Ge_{1.0}Sb_{2.2}Te_{3.5}$ (Table S1 and Fig. S2, ESI†), showing that these GST nanoplates are slightly Sb rich and Te poor.

To measure the electrical properties of the GST-124 nanoplates, a SiN_x membrane device was assembled. A single GST-124 nanoplate with a diagonal length of around 500 nm was spin-coated onto a SiN_x substrate and then was connected to a FIB-deposited platinum (Pt) line. A SiO_2 layer was deposited to prevent oxidation (Fig. 5a). FIB was used to accurately deposit Pt at a specified position, especially for such a small

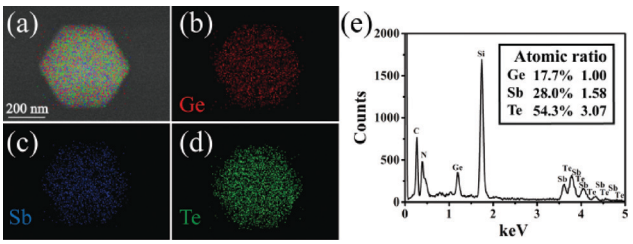

Fig. 4 (a–d) Elemental mapping images of a GST-124 nanoplate using EDS show that Ge, Sb, and Te elemental signals are overlaid (red for Ge, blue for Sb, and green for Te). (e) EDS spectrum of a single GST-124 nanoplate.

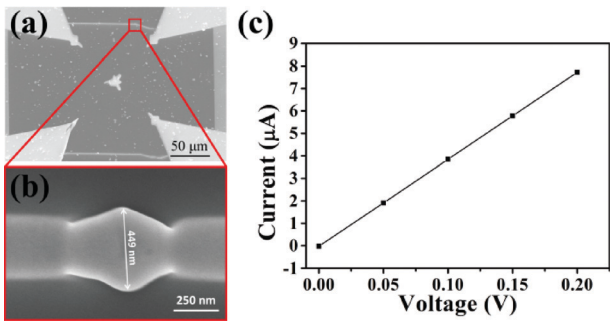

Fig. 5 (a) SEM image of a SiN_x membrane device. (b) Magnified SEM image of a single GST-124 nanoplate device connected to a FIB-deposited Pt line. (c) DC (*I*–*V*) sweep of a GST-124 nanoplate.

nanoscale device. A low intensity of the ion-beam was used to connect the GST-124 nanoplate to the Pt line (Fig. 5a).

The diagonal lengths of three GST-124 nanoplates in SiN_X membrane devices are 449, 542 and 502 nm (Fig. 5a and S3, ESI†), respectively. Eight DC (*I–V*) sweeps of different GST-124 nanoplates (Fig. 5c and S3 and S4†) show ohmic behavior with two-point probe resistance values in the same order of magnitude from 26 to 49 kohm, which indicates the crystalline state. However, crystalline GST compounds, especially for those having single phases along the pseudo-binary line, have a resistivity of about 1 mohm cm in hexagonal phase. The corresponding resistance is expected to be a few hundred ohms based on the value of 350 ohms computed from the approximate calculation of the electrical resistance for the crystal size as reported here (see Fig. S5† for more details). This inconsistency in excessive resistance is probably attributed to the contact resistance induced by the two-point probe method as previously reported by Meister *et al.*[25]

In conclusion, a solution route to synthesize colloidal GST-124 nanoalloys is reported, showing the first example of ternary PCM colloid nanomaterial synthesis in solution phase. The GST-124 nanoplates have uniform diagonal sizes, thicknesses, and compositions and are single crystalline with low electrical resistance, which may serve as new building block materials for nanoscale devices. Other ternary or even quaternary PCM nanomaterials might also be synthesized in solution, thus advancing the development of colloid materials chemistry.

Acknowledgements

H.-Y. Tuan acknowledges the financial support from the Ministry of Science and Technology through grants NSC 102-2221-E-007-023-MY3, MOST 103-2221-E-007-089-MY3, MOST 103-2622-E-007-025, and MOST 102-2633-M-007-002. W. W. W. acknowledges the support from the Ministry of Science and Technology through grant 103-2221-E-009-222-MY3.

Notes and references

1 F.-J. Fan, L. Wu and S.-H. Yu, *Energy Environ. Sci.*, 2014, **7**, 190–208.
2 M. A. Caldwell, S. Raoux, R. Y. Wang, H. S. Philip Wong and D. J. Milliron, *J. Mater. Chem.*, 2010, **20**, 1285–1291.
3 D. Aldakov, A. Lefrancois and P. Reiss, *J. Mater. Chem. C*, 2013, **1**, 3756–3776.
4 M. Dai, S. Ogawa, T. Kameyama, K.-I. Okazaki, A. Kudo, S. Kuwabata, Y. Tsuboi and T. Torimoto, *J. Mater. Chem.*, 2012, **22**, 12851–12858.
5 S.-H. Chang, B.-C. Chiu, T.-L. Gao, S.-L. Jheng and H.-Y. Tuan, *CrystEngComm*, 2014, **16**, 3323–3330.
6 V. A. Akhavan, B. W. Goodfellow, M. G. Panthani, C. Steinhagen, T. B. Harvey, C. J. Stolle and B. A. Korgel, *J. Solid State Chem.*, 2012, **189**, 2–12.
7 V. A. Akhavan, B. W. Goodfellow, M. G. Panthani, D. K. Reid, D. J. Hellebusch, T. Adachi and B. A. Korgel, *Energy Environ. Sci.*, 2010, **3**, 1600–1606.
8 W. Liu, D. B. Mitzi, M. Yuan, A. J. Kellock, S. J. Chey and O. Gunawan, *Chem. Mater.*, 2010, **22**, 1010–1014.
9 S. P. Hong, H. K. Park, J. H. Oh, H. Yang and Y. R. Do, *J. Mater. Chem.*, 2012, **22**, 18939–18949.
10 W. Zhang, H. Zeng, Z. Yang and Q. Wang, *J. Solid State Chem.*, 2012, **186**, 58–63.
11 K.-T. Yong, I. Roy, R. Hu, H. Ding, H. Cai, J. Zhu, X. Zhang, E. J. Bergey and P. N. Prasad, *Integr. Biol.*, 2010, **2**, 121–129.
12 Y. Jung, S.-H. Lee, D.-K. Ko and R. Agarwal, *J. Am. Chem. Soc.*, 2006, **128**, 14026–14027.
13 M. Ibanez, D. Cadavid, R. Zamani, N. García-Castelló, V. Izquierdo-Roca, W. Li, A. Fairbrother, J. D. Prades, A. Shavel, J. Arbiol, A. Pérez-Rodríguez, J. R. Morante and A. Cabot, *Chem. Mater.*, 2012, **24**, 562–570.
14 M. R. Buck, I. T. Sines and R. E. Schaak, *Chem. Mater.*, 2010, **22**, 3236–3240.
15 H.-Y. Tuan and B. A. Korgel, *Cryst. Growth Des.*, 2008, **8**, 2555–2561.
16 D. D. Vaughn, J. F. Bondi and R. E. Schaak, *Chem. Mater.*, 2010, **22**, 6103–6108.
17 M. H. Kim, G. Gupta and J. Kim, *RSC Adv.*, 2013, **3**, 288–292.
18 I. U. Arachchige, R. Soriano, C. D. Malliakas, S. A. Ivanov and M. G. Kanatzidis, *Adv. Funct. Mater.*, 2011, **21**, 2737–2743.
19 S. Schulz, S. Heimann, K. Kaiser, O. Prymak, W. Assenmacher, J. T. Brüggemann, B. Mallick and A.-V. Mudring, *Inorg. Chem.*, 2013, **52**, 14326–14333.
20 I. Friedrich, V. Weidenhof, W. Njoroge, P. Franz and M. Wuttig, *J. Appl. Phys.*, 2000, **87**, 4130–4134.
21 K. Perumal, W. Braun, H. Riechert and R. Calarco, *J. Cryst. Growth*, 2014, **396**, 50–53.
22 M. Schuck, S. Rieß, M. Schreiber, G. Mussler, D. Grützmacher and H. Hardtdegen, *J. Cryst. Growth*, 2015, **420**, 37–41.
23 S. Song, D. Yao, Z. Song, L. Gao, Z. Zhang, L. Li, L. Shen, L. Wu, B. Liu, Y. Cheng and S. Feng, *Nanoscale Res. Lett.*, 2015, **10**, 89.
24 B. J. Kooi and J. T. M. De Hosson, *J. Appl. Phys.*, 2004, **95**, 4714–4721.
25 S. Meister, D. T. Schoen, M. A. Topinka, A. M. Minor and Y. Cui, *Nano Lett.*, 2008, **8**, 4562–4567.

